Journal of
Materials Chemistry B

Accepted Manuscript

This article can be cited before page numbers have been issued, to do this please use: M. Wang, Y. Li, J. Cao, M. Gong, Y. Zhang, X. Chen, M. Tian and H. Xie, *J. Mater. Chem. B*, 2017, DOI: 10.1039/C7TB00517B.

ROYAL SOCIETY OF CHEMISTRY

rsc.li/materials-b

View Article Online
DOI: 10.1039/C7TB00517B

Accelerating effects of genipin-crosslinked small intestinal submucosa for defected gastric mucosa repair

Min Wang, Yan-Qing Li, Jie Cao, Mei Gong, Yi Zhang, Xi Chen, Mao-Xuan Tian and Hui-Qi Xie*

Laboratory of Stem Cell and Tissue Engineering, Regenerative Medicine Research Center, State Key Laboratory of Biotherapy, West China Hospital, Sichuan University, Chengdu 610041, P.R. China. *Email: xiehuiqi@scu.edu.cn ; Tel/Fax: +86-28-85164088

View Article Online
DOI: 10.1039/C7TB00517B

Abstract

The slow healing of gastric mucosa defects caused by endoscopic surgery is a common but severe clinical problem for the lack of effective treatment. Small intestinal submucosa (SIS) is a bio-derived extracellular matrix scaffold with remarkable repair ability for soft tissue, but its rapid degradation and poor mechanical properties in stomach environment limit its application for gastric mucosa regeneration. Herein, we modified SIS by genipin, a natural crosslinking agent, to improve its resistance against degradation in gastric juice and to promote the healing of gastric mucosa defects. The crosslinking characteristics of genipin-crosslinked SIS (GP-CR SIS) were evaluated by crosslinking degree, swelling ratio and FITR respectively. GP-CR SIS was highly resistant to gastric juice digestion and had a great increase in mechanical properties. Additionally, GP-CR SIS maintained excellent biocompatibility according to the cytotoxicity test, hemolysis test and rat subcutaneous implant assay. In *in vivo* study we treated defected gastric mucosa with GP-CR SIS in a rabbit endoscopic submucosal dissection (ESD)-related ulcer model. After two weeks of surgical treatment, GP-CR SIS significantly expedited wound closure and ameliorated newly constructed tissue by providing protective microenvironment for rapid granulation tissue formation and accelerating angiogenesis/re-epithelialization. In conclusion, this study demonstrated the great therapeutic potential of GP-CR SIS scaffolds in accelerating defected gastric mucosa regeneration.

Keywords: small intestinal submucosa, genipin, crosslinking, gastric mucosa repair

View Article Online
DOI: 10.1039/C7TB00517B

Introduction

Endoscopic submucosal dissection (ESD) is popularly accepted as an alternative to open surgery for the treatment of gastric lesions due to its relatively noninvasive property and its superiority in providing en bloc specimens for pathology evaluation compared to other endoscopic methods [1]. Nevertheless, the complications accompanied by ESD are serious, especially bleeding and perforation. The frequency of bleeding associated with ESD was reported up to 38%. In spite of lower incidence (4%), the perforation was more likely to bring a greater risk for significant morbidity and mortality [2, 3]. With no effective preventions or therapies, ESD-induced defected areas exposed to corrosive gastric juice may induce the slow-healing of gastric mucosa, which put patients suffering from the complication at higher risk. Therefore it is necessary to protect the lesion from gastric juice, and promote the gastric mucosa regeneration.

Small intestinal submucosa (SIS), as an acellular matrix tissue engineering material, has been widely used in scientific and clinical fields due to its good biocompatibility, biodegradability and low immunogenicity [4, 5]. The composition of SIS is mainly collagens, with a wide variety of growth factors, including VEGF, TGF, bFGF, EGF as well as glycosaminoglycans, heparins, and hyaluronic acids [6-8]. SIS has been broadly applied for the repair of various tissues and organs, such as heart, bladder, urethra, biliary tract, and skin [9-13]. However, the application of SIS for gastric tissue repair was extremely limited due to its rapid degradation and poor mechanical properties when exposed to the extremely acidic (pH=1.2) and pepsin-riched gastric juice. Hence, the modification of SIS is necessary for its application in gastric tissue repair.

Two strategies, the physical crosslinking method and the chemical crosslinking method, have been widely used in the modification of bio-derived materials. Physical crosslinking methods do

View Article Online
DOI: 10.1039/C7TB00517B

not cause potential cytotoxic harm, but the low crosslinking efficiencies make them difficult to meet the desired crosslinking degree. Many chemical crosslinking agents including the aldehydes (formaldehyde, glutaraldehyde, glyceraldehyde), epoxy compounds and carbodiimides are efficient in crosslinking, but the side-effects, including high cytotoxicity, calcification, and mismatched mechanical properties restrict their further utilization in clinics [14-16]. It is, therefore, required to provide an alternative crosslinking agent with low cytotoxicity and the ability to form stable and biocompatible crosslinking product for the modification of SIS. Genipin, a natural compound isolated from the fruits of *Gardenia jasminoides* Ellis, has been used as a crosslinker to fix various natural biomaterials such as collagenous tissues, chitosan, gelatin, and fibrinogen scaffolds [17-20]. Compared with conventional synthetic crosslinker glutaraldehyde, genipin possesses corresponding crosslinking capability but markedly lower cytotoxicity and better biocompatibility [21]. Additionally, genipin crosslinking remarkably enhances the resistance against enzymatic degradation in various nature-derived biomaterials such as porcine pericardia, bovine pericardia and porcine corneal stroma [22-24].

In this study, we evaluated the therapeutic effect of genipin-crosslinked SIS (GP-CR SIS) in accelerating gastric mucosa regeneration. SIS was crosslinked with genipin to improve its resistance against degradation in corrosive gastric juice, and then was examined by crosslinking characteristics. Meanwhile, the biocompatibility of GP-CR SIS was assayed by cytotoxicity, hemolysis, and histocompatibility. The healing rate of gastric mucosa defects repaired with GP-CR SIS was assessed by macroscopic observation and histological examinations in a rabbit ESD-related ulcer model. In addition, the possible mechanism of GP-CR SIS in accelerating gastric mucosa regeneration was explored in terms of promoting vascularization and

View Article Online
DOI: 10.1039/C7TB00517B

epithelialization.

Experimental

Preparation of GP-CR SIS

SIS was prepared following the multi-step method described previously [25]. In brief, the serosa, tunica muscularis and tunica mucosa of fresh porcine jejunum were manually removed by a spatula. Subsequently, the submucous membrane was degreased by immersing into the organic solvent (methanol and chloroform, V/V=1:1) for 12 h. Then the membranes were decellularized in 0.05% trypsin for 12 h, and in 0.5% sodium dodecylsulphate (SDS) for 4 h. Finally the SIS sheets were disinfected by soaking in 0.1% peracetic acid, and frozen-dried by lyophilizer.

For genipin crosslinking, SIS was immersed in various genipin (ConBon, Chengdu, China) concentrations (0.05, 0.1, 0.3, and 0.5%, wt %) buffered with phosphate buffer saline (PBS) at 37 $^{\circ}$C for 24 h with continuous shaking. Then the samples were rinsed five times (3 min each rinse) in deionized water. Finally, the GP-CR SIS scaffolds were obtained by lyophilization again.

Crosslinking degree

The crosslinking degree of GP-CR SIS, defined as the percentage of free amino groups in SIS reacted with genipin subsequent to fixation, was determined by ninhydrin assay [26]. In brief, the lyophilized samples (~5 mg, n=3) were heated with a ninhydrin solution at 100 $^{\circ}$C for 20 min. After cooling to room temperature, the optical absorbance of each solution was recorded with a spectrophotometer (Hach, USA) at a wavelength of 570 nm using glycine at various known concentrations as standard. The crosslinking degree was then calculated by following the equation:

View Article Online
DOI: 10.1039/C7TB00517B

Crosslinking degree= [(NH reactive amine) $_{fresh}$-(NH reactive amine) $_{fixed}$] / (NH reactive amine)

$_{fresh}$ × 100

Where fresh and fixed are the mole fractions of free NH_2 remaining in SIS and GP-CR SIS scaffolds, respectively.

Swelling ratio

Swelling ratio studies were carried out according to Nakatsuka S et al. with slight modifications [27]. Briefly, the lyophilized samples (20 mm × 20 mm, n=3) were weighed in the dried state and then immersed in 10 ml PBS (pH=7.4) at 37 °C for 1, 3, 6, 12, 24 h. Subsequently, the wet weight was determined by gently blotting the swollen film with filter paper to remove excess water. The swelling ratio was calculated as follows:

$$S_w(\%) = (W_s - W_i) / W_i \times 100\%$$

Where S_w is the swelling ratio of the test sample, W_i is membrane initial dried weight and W_s is the weight of swollen material.

Morphology and biochemical change

The surface morphologies of SIS and GP-CR SIS scaffolds were examined by scanning electron microscopy (SEM). The samples were coated with gold and then observed under SEM (JSM-6500LV, Jeol, Japan). For biochemical compositions and crosslinking mechanisms, FTIR was performed on Nicolet 6700 FTIR (Thermo, USA) with a Smart Endurance Diamond attenuated total reflectance (ATR) accessory on each sample. The spectra were collected by co-adding 64 scans in the spectral region of 4000-650 cm^{-1} at a resolution of 2 cm^{-1}. The spectra

View Article Online
DOI: 10.1039/C7TB00517B

were ATR collected and displayed as absorbance spectra. Comparisons were made between SIS and GP-CR SIS scaffolds to study the effect of genipin crosslinking condition.

In vitro degradation

To mimic the gastric environment, simulated gastric fluid (SGF) was used in the degradation test *in vitro*. According to the USP Convention, SGF was prepared with 0.32 % (w/v) porcine pepsin in 0.2% NaCl at pH=1.2. The circular aseptic test samples (diameter=15 mm) were well immersed in SGF and maintained in 5% CO_2 at 37 $^{\circ}$C and SGF was replaced every two days. At predetermined time points (2w, 4w and 8w), the samples were taken out and then washed with distilled water, followed by being lyophilized for 48 h. The residue weight ratio of the samples was calculated as the residue mass divided by the original weight.

Mechanical property

In the mechanical properties measurement, the samples treated by SGF at predetermined time points were taken out and washed with distilled water, followed by being lyophilized for 48 h. Then the ultimate tensile strength and stiffness of rectangle samples (10 mm × 40 mm, n=6) before (0w) and after SGF treatment (2w, 4w and 8w) were determined in dry conditions using a uniaxial testing machine (Instron 8874) equipped with a 10 kN load cell at a crosshead displacement speed of 10 mm/min.

Cytotoxicity test

The cytocompatibility of GP-CR SIS was determined by both direct and indirect cytotoxicity

View Article Online
DOI: 10.1039/C7TB00517B

assay. For direct cytotoxicity assay, human gastric mucosal epithelial cell line GES-1 was seeded on the surface of the scaffolds and cultured for 72 h in complete medium comprised of Dulbecco's modified eagle medium-high glucose (Gibco, USA) supplemented with 10% fetal bovine serum (Gibco, Australia) and 100 U/ml of penicillin and 0.1 mg/ml streptomycin (Thermo, USA).The cells were stained with calcein AM solution (2 μM, Sigma, USA) to display the live cell morphology and GP-CR SIS was presented with autofluorescence [28]. Then the samples were observed using a confocal laser scanning microscope (CLSM, Nikon, Japan) at excitation wave-length of 488 nm and 638 nm.

The indirect cytotoxicity test was carried out according to ISO 10993: 2007. The extract was prepared using complete medium with an extracting vehicle volume to material surface area ratio 1: 6 in a humidified atmosphere with 5% CO_2 at 37 $^{\circ}$C for 24 h. The complete medium and a 0.64% solution of phenol in the complete medium were used as negative control and positive control respectively. The GES-1 cells were seeded in 96-well cell culture plates at 4×10^3 cells/well. After cell attachment, the culture medium was replaced by corresponding extract, and changed every two days. After incubating for 1, 3 and 5 days, cells viability was tested by MTT assay. The optical density (OD) of absorbance at 490 nm was measured and relative growth rate (RGR) was calculated by the following equation:

$$RGR\ (\%) = OD_s / OD_{nc} \times 100\%$$

Where OD_s and OD_{nc} are the optical densities of the tested samples and the negative control group, respectively. And the RGR of each group was converted into cytotoxicity grades according to ISO 10993: 2009.

View Article Online
DOI: 10.1039/C7TB00517B

Hemolysis test

The hemolysis test was performed according to the ISO standard 10993: 2009. Briefly, the sample extracts (n=3) were prepared by soaking 30 cm^2 sample in a glass tube containing 5 ml normal physiological saline and kept at 37 $^{\circ}C$ for 24 h. Distilled water and normal physiological saline served as positive and negative control respectively. After that, 8 ml freshly collected venous blood of a healthy adult New Zealand white rabbit was diluted with 10 ml normal physiological saline containing 0.5 ml potassium oxalate anticoagulant (20 g/L). Then 0.2 ml diluted blood was added into the tube and maintained at 37 $^{\circ}C$ for 60 min. After incubation, samples were centrifuged and the optical density (OD) of supernatant was measured at the wavelength of 545 nm. The hemolysis ratio (HR) was calculated according to the following equation:

$$HR\ (\%) = [(OD_t - OD_n) / (OD_p - OD_n)] \times 100\%$$

Where OD_t, OD_n and OD_p mean optical densities of the samples, negative control and positive control groups respectively. The test material with the percentage of more than 5% was considered as hemolytic.

Animal study

All animal experimental procedures have been approved by Sichuan University Animal Care and Use Committee in concordance with the Principles of Laboratory Animal Care formulated by the National Society for Medical Research.

For subcutaneous implant, twelve male Sprague-Dawley rats weighting 200-220 g were purchased from the Laboratory Animal Academy of Sichuan Medical Sciences Institute. Briefly,

View Article Online
DOI: 10.1039/C7TB00517B

five separate skin incisions were made on the back of the rats. Then subcutaneous pockets were created, large enough with a blunt dissection to match the sample. Square SIS and GP-CR SIS scaffolds (10 mm × 10 mm) were carefully set into each pocket and skin was routinely closed. Following euthanasia, the rats (three per time point) were sacrificed via cervical dislocation at the predetermined end time points (1, 2, 4 and 8 week). Then the scaffolds and adjacent surrounding tissues were collected. Thereafter the retrieved implants were either fixed in 4% paraformaldehyde solution for subsequent histological evaluation or snap frozen for succedent atomic absorption analysis.

For gastric mucosa repair, fifty-four New Zealand white rabbits weighting 2.5-2.8 kg were purchased from the Laboratory Animal Academy of Sichuan Medical Sciences Institute. To simulate the formation and properties of defected gastric tissue caused by endoscopic surgery, the endoscopic submucosal dissection (ESD)-related ulcer model was used in gastric mucosa repair [29]. The rabbits were divided into three groups randomly (Control, SIS and GP-CR SIS; n=18 each). In brief, the stomach was exposed by an upper ventral midline incision and opened in line with the greater curvature. Then 6% hydroxyethyl starch was injected into the submucosa to separate mucosa from muscularis. An acute gastric ulcer with diameter of about 12 mm was created by resecting the swollen mucosal layer with microsurgical instruments. A circular scaffold (SIS or 0.5%GP-CR SIS, diameter=20 mm) were used to cover the defected area and tightly fixed with non-absorbable suture **(Fig.S1).** The untreated ulcer served as the control group. Following euthanasia at 1, 3, 7, 14 or 28 d post-implantation, the stomach was excised en bloc. After taken by a digital camera and stereomicroscope for macroscopic observation, the samples were fixed in paraformaldehyde for histological analysis or snap frozen for molecular analysis.

View Article Online
DOI: 10.1039/C7TB00517B

Histological study

Hematoxylin and eosin (H&E) staining was used to observe the biocompatibility of scaffolds after subcutaneous implantation in rats. Inflammatory cells were identified at the implant site based on their respective morphologies from high powered fields (HPFs, n=6) with a digital image analysis system (Nikon, Japan) [30]. Then the number of inflammatory cells was quantified with a computer-based image analysis system (Image-Pro Plus, USA).

To analyze the repair of mucosal defects, rabbit gastric tissues were performed with H&E staining to observe the structures of gastric wall. Periodic acid Schiff (PAS) staining was used to evaluate the expression of mucosal glycoproteins. Furthermore, immunohistochemistry and immunofluorescence staining was used to detect the gastric epithelial cells (CK18, Santa, USA), blood vessels (CD31, Bioss, China) and proliferating cells (Ki67, Dako, USA). The density of blood vessels in granulation tissue and proliferating epithelial cells in ulcer margin were quantified from three random HPFs of samples (n=3 in each group) on day 7.

RT-qPCR

Briefly, total RNA from ulcer tissue was extracted with Trizol protocol (Takara, Japan) and then was reverse-transcribed into cDNA using GoScript™ Reverse Transcription reagent kit (Takara, Japan). The relative gene expression levels were detected by quantitative RT-qPCR using SYBR Green 1 PCR master mix (Takara, Japan) and Lightcycler 96 system (Roche, Switzerland). The primers used were shown in **Table S1**. The results of the RT-qPCR were performed by the $2^{-\delta\delta ct}$ method.

View Article Online
DOI: 10.1039/C7TB00517B

Western blot

The frozen gastric tissue was homogenized in the RIPA buffer supplemented with PMSF using bead mill homogenizer. After the determination of protein concentration, equal amounts of total protein were electrophoresed in 8% w/v SDS-polyacrylamide gel. Then the separated bands were transferred to PVDF membrane. The blots were probed with the following primary antibody: VEGFR2 (Abbiotec, USA), ANGPT2 (Santa, USA), COX2 (Cayman, USA) and followed by incubation with secondary antibodies (Cwbiotech, China). The membranes were then reacted with Immobilon western kit (Millipore, USA). GAPDH served as internal control.

Statistical analysis

All of the data were presented as the mean ± standard deviation (SD). ANOVA was performed to analyze the data of multiple comparisons. $P < 0.05$ was considered significantly.

Results

Crosslinking characteristics

The crosslinking characteristics of GP-CR SIS scaffolds were determined by crosslinking degree, swelling ratio, ATR-FTIR and SEM **(Fig.1)**. The color of SIS became dark-bluish after crosslinking and gradually deepened with increased genipin concentration **(Fig.1D)**. As presented, the crosslinking degrees of GP-CR SIS were all above 65% after fixation **(Fig. 1A)** and the swelling ratio significantly decreased, even at the 0.05% genipin concentration. As shown in **Fig. 1B**, the swelling ratio of SIS almost reached a plateau after a soaking period of 6 h. In comparison,

View Article Online
DOI: 10.1039/C7TB00517B

the swelling ratios of GP-CR SIS kept constant after 3 h of soaking, and attenuated to 120-170%, about one half of SIS group. To further explore the reactive groups in crosslinking we attained the ATR-FTIR. The spectrum of SIS showed the characteristic bands of amide I and amide II, respectively at 1633 cm^{-1} and 1549 cm^{-1}, and that of amide III at 1235 cm^{-1}, caused by C-N stretching vibrations, amide N-H in-plane bending vibrations and CH_2 wagging vibrations. Bands due to N-H and O-H stretching vibrations overlapped in the adsorption peak at 3306 cm^{-1}. Compared with SIS, the spectra of GP-CR SIS scaffolds showed a decrease in the characteristic peak of amine ($-NH_2$) stretch at 1549 cm^{-1}, which was slightly decreased with increased concentration of genipin (**Fig. 1C**). Although genipin efficiently fixed SIS, it had almost no effects on the ultrastructure of SIS. SEM results presented that all GP-CR SIS scaffolds had a porous structure with bundles of crimped collagen fibers at the submucosal surface **(Fig. 1D)**.

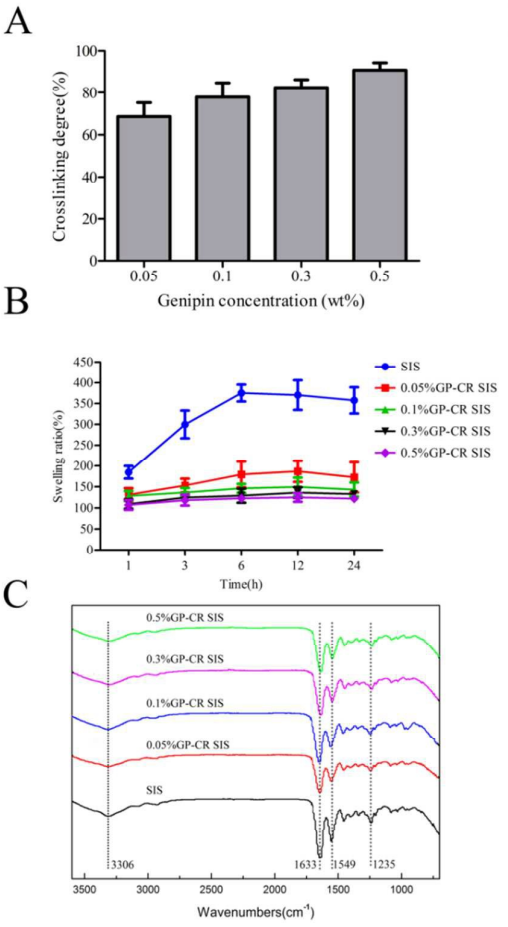

View Article Online
DOI: 10.1039/C7TB00517B

Fig.1. Genipin efficiently fixed SIS at various known concentrations after a 24-h crosslinking treatment.

A. Crosslinking degrees of GP-CR SIS fixed at various genipin concentrations; B. Swelling ratios of GP-CR SIS fixed at various genipin concentrations. C. ATR-FTIR spectra of SIS and GP-CR SIS. D. Macroscopic observation of SIS and GP-CR SIS (left column); SEM photographs of SIS and GP-CR SIS (right column); SEM Scale bar: 50 μm.

Resistance against SGF degradation

The resistance against degradation in gastric juice of GP-CR SIS was determined in SGF *in vitro*. All GP-CR SIS scaffolds remained intact during the 8-week digestion by SGF, accompanied by the loss of color **(Fig.2C).** The residual mass ratios of GP-CR SIS scaffolds were all more than 90% at the end of the 8-week incubation period **(Table 1)**. In contrast, complete degradation of untreated SIS occurred after immersing in SGF within 24 h.

The mechanical properties as the important parameter of GP-CR SIS scaffolds were also detected before and after immersing in SGF. As shown in **Fig.2A**, genipin crosslinking statistically increased the ultimate tensile strength of SIS ($P < 0.05$). However, the ultimate tensile strength of GP-CR SIS scaffolds displayed a remarkable decrease, declining to about one fifth of its original one after a 2-week immersion in SGF and the values were comparable. Over the subsequent 6 weeks, there was little variation in ultimate tensile stress. While there was no significant difference between SIS and GP-CR SIS in stiffness, the treatment of SGF had almost no effect on the stiffness of GP-CR SIS in 8-week incubation **(Fig. 2B)**. The mechanical data of the untreated SIS was not available on account of the complete degradation within 24 h. These results also

View Article Online
DOI: 10.1039/C7TB00517B

demonstrated that GP-CR SIS had improved resistance against SGF degradation.

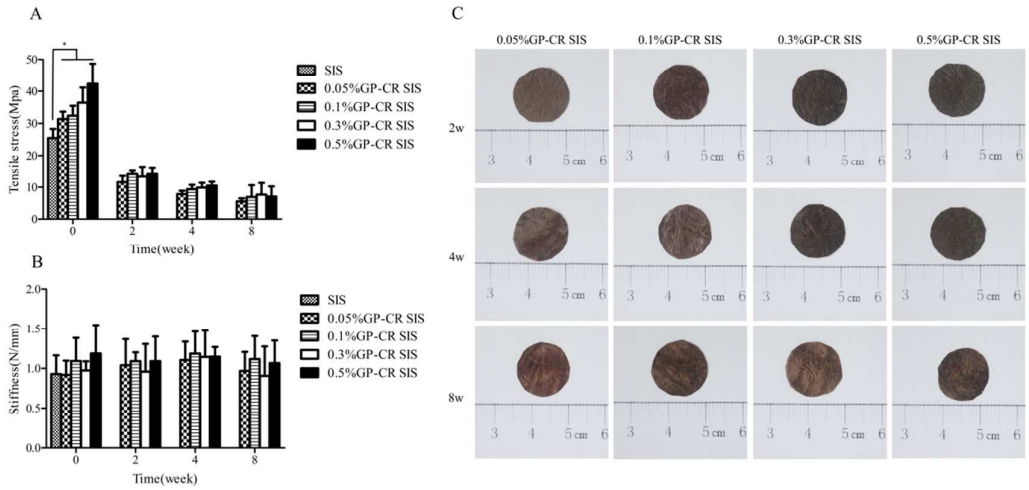

Fig.2. Genipin crosslinking enhanced the mechanical property and the resistance of SIS against degradation in SGF.

A. Tensile stress of SIS and GP-CR SIS before (0 w) and after treatment with SGF for 2, 4 and 8 weeks. *: Significantly different from SIS ($P < 0.05$). B. Stiffness of SIS and GP-CR SIS before (0 w) and after treatment with SGF for 2, 4 and 8 weeks. C. Representative macroscopic images of GP-CR SIS scaffolds collected at week 2, 4 and 8 after immersion in SGF.

Table 1

Residual mass ratio of GP-CR SIS scaffolds after treatment with SGF

group	2 week	4 week	8 week
0.05%GP-CR SIS	95.31±1.00%	92.99±0.71%	90.83±0.92%
0.1%GP-CR SIS	93.77±0.46%	91.97±0.52%	91.00±0.34%
0.3%GP-CR SIS	95.62±0.88%	94.92±0.68%	93.16±0.35%
0.5%GP-CR SIS	94.94±0.65%	94.13±1.00%	92.34±0.30%

View Article Online
DOI: 10.1039/C7TB00517B

Biocompatibility of GP-CR SIS

The cytocompatibility of GP-CR SIS was evaluated by both direct and indirect cytotoxicity assay. As shown in **Fig. 3C**, SIS and GP-CR SIS scaffolds were filled with GES-1 cells, which displayed a spread shape on the surface of the scaffolds. For indirect cytotoxicity assay, the GES-1 cells were cultured in SIS or GP-CR SIS extract. As prolonging the culture time, the OD readings increased remarkably in negative, SIS and GP-CR SIS groups, in contrast the positive group stayed at its initial minimum value all the time **(Fig. 3A)**. This indicated that the extract of SIS and GP-CR SIS scaffolds has no inhibition on the proliferation of GES-1 cells. The corresponding RGR and toxicity grade of different extracts at different times are listed in **Table 2**. After 1, 3 and 5 days' incubation, the RGR of GP-CR SIS scaffolds was in the range 103.10-136.96%, significantly higher than that of SIS ($P < 0.05$), and their corresponding cell toxicity grades were all grade 0 during the incubation.

As shown in hemocompatibility, the supernatant of SIS and GP-CR SIS was clear with red blood cells sedimented on the bottom of the tubes **(Fig.S2)**, indicating no hemolysis as negative group. In contrast, the supernatant of positive group was reddish with no sedimented RBC, indicating total hemolysis. The OD values of SIS and GP-CR SIS were all below 5% **(Table 3)**. So GP-CR SIS did not lead to erythrocytes according to the ISO standard.

A set of representative H&E-stained histological sections of scaffolds harvested at 2 and 8 weeks post-implantation were shown in **Fig. 3D.** At 2 weeks after implantation, both SIS and GP-CR SIS scaffolds remained relative intact structures and the inflammatory response surrounding SIS was more severe than GP-CR SIS. However, SIS was almost completely degraded after 8-week postoperatively while GP-CR SIS scaffolds still remained. To further

View Article Online
DOI: 10.1039/C7TB00517B

evaluate the histocompatibility, the number of inflammatory cells surrounding scaffolds was quantified **(Fig. 3B)**. At 1 and 2-week postoperatively, the number of inflammatory cells in SIS group was significantly higher than that in GP-CR SIS group ($P < 0.05$), and then dramatically declined at 4 and 8 weeks. In contrast, the inflammatory cells of GP-CR SIS, which mainly located at the surface of the scaffolds, were steadily few during the 8-week period, presenting a relatively mild reaction.

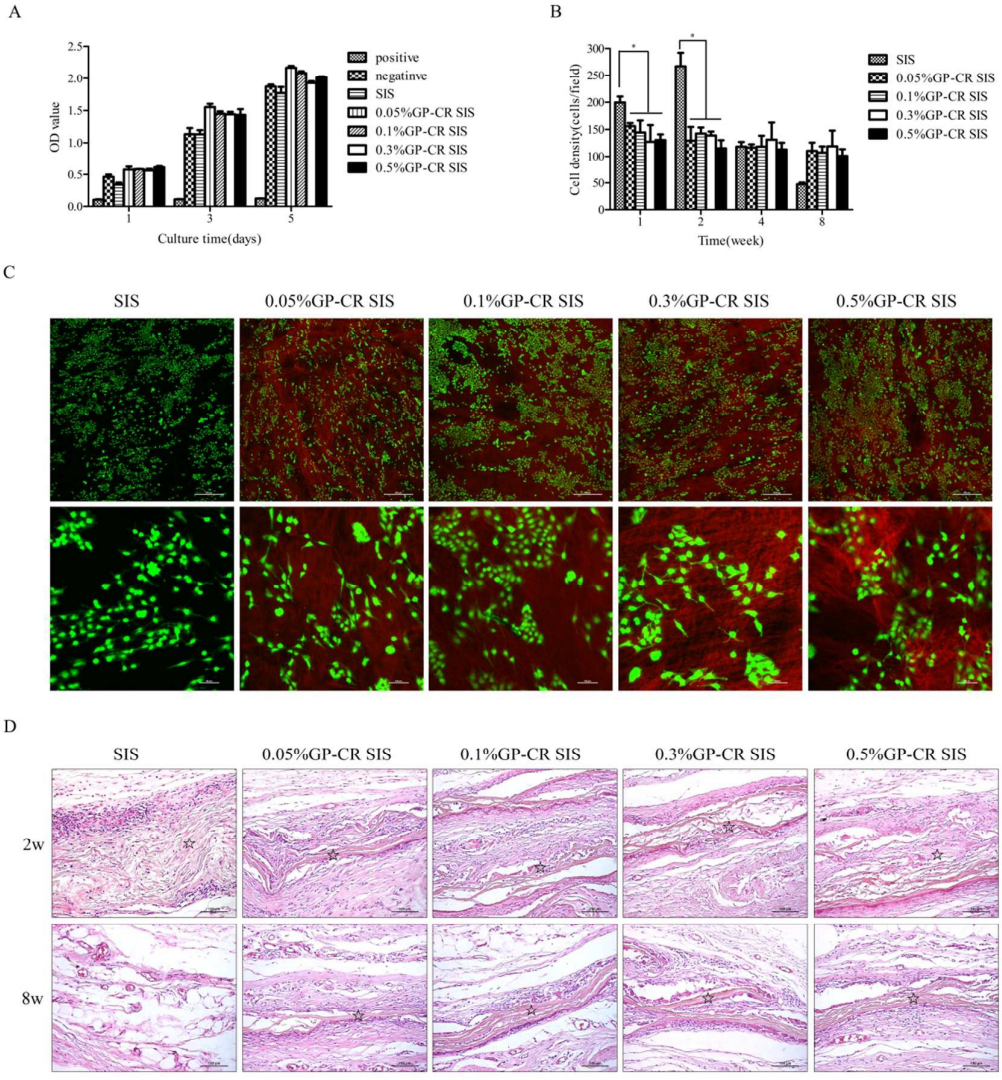

View Article Online
DOI: 10.1039/C7TB00517B

Fig.3. The cytocompatibility and histocompatibility of GP-CR SIS.

A. GES-1 cell viability estimated by MTT assay after 1, 3, and 5 days' incubation in different extracts. B. Densities of inflammatory cells in tissues implanted with different scaffolds retrieved at distinct durations postoperatively. *: Significantly different from SIS group ($P < 0.05$). **C.** CLSM photographs of the morphology of GES-1 cells after cultured on the scaffolds for 3 days. Live cells were stained with calcein AM (green) and GP-CR SIS was viewed by its auto-fluorescence (red). Scale bar：500 μm (upper panel); Scale bar: 100 μm (lower panel). D. Representative H&E-stained photographs of GP-CR SIS scaffolds retrieved at 2-week (upper panel) and 8-week (lower panel) postoperatively. ☆ indicates scaffolds. Scale bar: 100 μm.

Table 2

The RGR and toxicity of SIS and GP-CR SIS scaffolds

Group	1 day		3 day		5 day	
	RGR (%)	Grade	RGR (%)	Grade	RGR (%)	Grade
positive	22.82	4	9.90	4	6.64	4
Negative [a]	100.00	0	100.00	0	100.00	0
SIS [a]	73.79	2	99.85	1	94.64	1
0.05%GP-CR SIS[a b]	124.69	0	136.96	0	115.87	0
0.1%GP-CR SIS[a b]	125.63	0	127.64	0	111.40	0
0.3%GP-CR SIS[a b]	121.53	0	126.91	0	103.10	0
0.5%GP-CR SIS[a b]	132.40	0	126.29	0	107.64	0

a: Significantly different from the positive group ($P < 0.01$).

b: Significantly different from SIS group ($P < 0.05$).

View Article Online
DOI: 10.1039/C7TB00517B

Table 3

The hemolysis of SIS and GP-CR SIS scaffolds

Group	OD value (mean±SD)	Hemolysis (%)
Positive group	0.5760±0.0095	100
Negative group	0.0057±0.0032	0
SIS	0.0154±0.0067	3.54
0.05%GP-CR SIS	0.015±0.0084	1.71
0.1% GP-CR SIS	0.0158±0.0087	1.77
0.3% GP-CR SIS	0.0141 ±0.0083	1.47
0.5% GP-CR SIS	0.0114±0.0042	1.00

Macroscopic observation and histological analysis of wound healing

For in *vivo study,* 0.5% GP-CR SIS was selected in ESD-related ulcer repair for its own anti-Helicobacter pylori property (**Fig.S5**) and the high crosslinking efficiency among GP-CR SIS scaffolds. The healing progress of defected area was closely followed at predetermined time points **(Fig. 4, Fig. S3)**. Two rabbits in control group died from gastric perforation within one week after operation, while there were no serious complications in SIS and GP-CR SIS groups throughout the experiment. Stereomicroscopic pictures clearly showed that after 7 days, the largest defected area remained in the control group, followed by SIS and GP-CR SIS groups **(Fig4.B)**. The gastric defected area had almost closed 14 days after treatment with GP-CR SIS while in the other two groups the lesions were still obvious **(Fig.4A)**. The wounds of control and SIS groups did not completely heal up even on day 28. According to the wound areas measured at different time

View Article Online
DOI: 10.1039/C7TB00517B

points, GP-CR SIS prominently accelerated wound healing on day 7 compared to SIS and control groups **(Fig.4 A).**

As shown in histological results, lesions treated with GP-CR SIS were covered with successive layers of neoepithelial cells on day 14 while the granulation tissue of the other two groups remained exposed **(Fig.4D)**. In spite of the full coverage of gastric mucosa, the thickness of mucosa in control group was still lower than the uninjured mucosa at day 28, while the thickness of mucosa in GP-CR SIS group was higher than the normal mucosa **(Fig.4C).** Immunohistochemical staining results showed that cells covering the granulation tissue in all groups were almost positive for CK18, a specific marker of gastric epithelial cell, indicating the regeneration of gastric mucosa epithelium at defected sites **(Fig.4E)**. However, the epithelium arranged more orderly in GP-CR SIS group than in the other two groups. Neutral mucosubstances such as glycoproteins were clearly detected by PAS staining in GP-CR SIS treated group **(Fig.4E)**, demonstrating the function recovery of gastric mucosa epithelium in the healing areas.

View Article Online
DOI: 10.1039/C7TB00517B

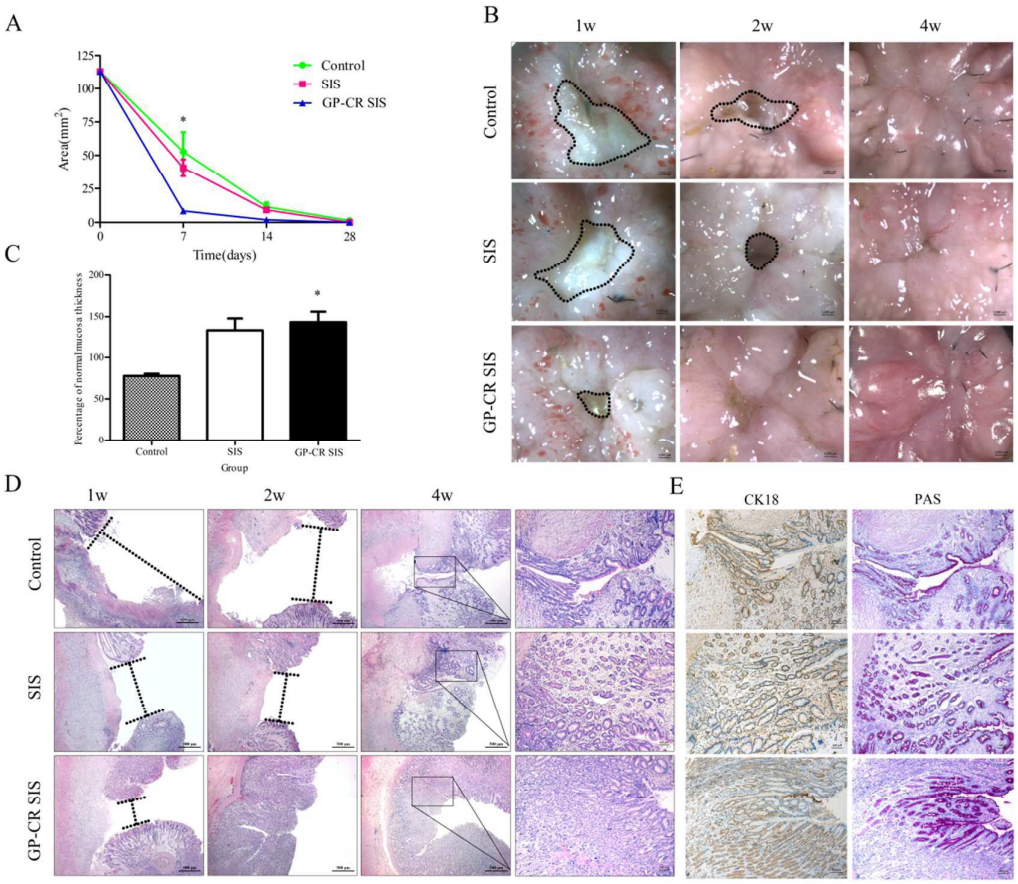

Fig.4. GP-CR SIS promoted defected gastric mucosa healing in *in vivo* models.

A. Quantification of wound areas on days 0, 7, 14, and 28 post operation. *: Significantly different from the control and SIS groups at day 7 ($P < 0.05$). B. Representative macroscopic images of wounds collected at day 7, 14 and 28 by stereomicroscope. Scale bar: 1000 μm. C. Relative thickness percentage of regenerated gastric mucosa to normal gastric mucosa on day 28. *: Significantly different from the control group ($P < 0.05$). D. Representative H&E staining images of wounds collected at day 7, 14 and 28. Scale bar: 500 μm (the first three columns); Scale bar: 100 μm (the last column). E. Representative CK18 immunohistochemical staining images (left column) and PAS staining images (right column) of wounds collected at day 28. Scale bar: 100 μm.

View Article Online
DOI: 10.1039/C7TB00517B

Angiogenesis and epithelium proliferation in gastric mucosa healing

According to the immunohistochemical labelling for CD31, the number of blood vessels in granulation tissue of GP-CR SIS group was higher than that in control and SIS groups at day 7 (**Fig.5A and B,** $P < 0.05$)**.** In PCR results, the expression of VEGFR2 and ANGPT2, two major angiogenic regulatory genes, significantly increased in GP-CR SIS group compared with control group at day 1 and 7 **(Fig.5C**, $P < 0.05$**)**. For SIS treatment, both VEGFR2 and ANGPT2 expression levels were higher than control group at day1, but returned to levels of control group at day 3 and 7. The protein levels of VEGFR2 and ANGPT2, measured by Western blot, were consistent with the results of their gene expression **(Fig.5D).**

As for the immunofluorescent staining of Ki67, the number of proliferating epithelial cells in the ulcer margin of GP-CR SIS group increased at day 7 and attained significance compared to levels in the control and SIS groups **(Fig.5A and B**, $P < 0.05$**)**. Additionally, the gene and protein expression of COX2 was significantly higher in GP-CR SIS group compared with control and SIS groups at day 1 and 3 **(Fig.5C and D).** However, the treatment with SIS and GP-CR SIS did not affect EGFR levels at any time point **(Fig.5C).**

View Article Online
DOI: 10.1039/C7TB00517B

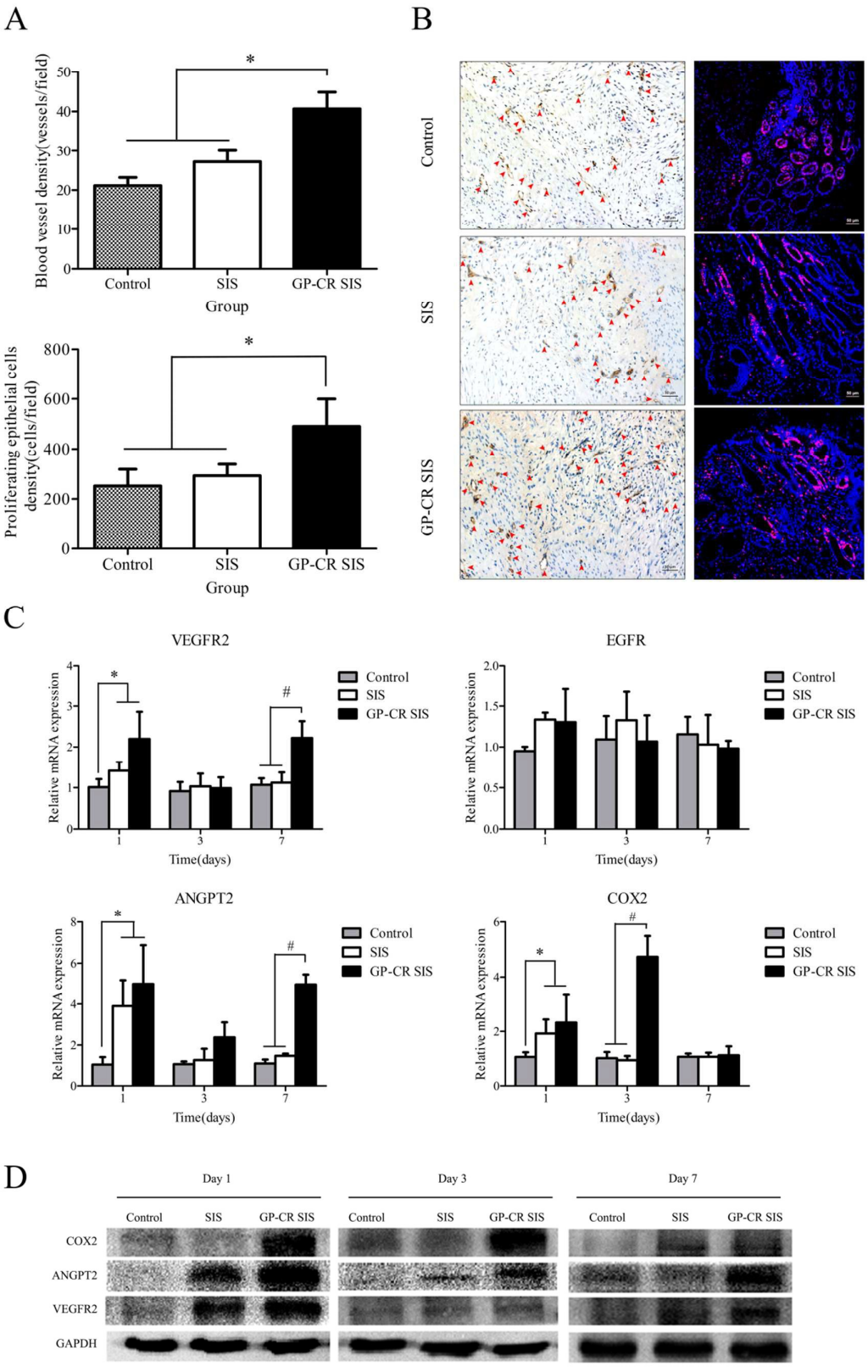

View Article Online
DOI: 10.1039/C7TB00517B

Fig.5. GP-CR SIS enhanced the angiogenesis and epithelium proliferation in gastric mucosa regeneration.

A. Quantification of the number of vessels in the granulation tissue (upper panel) and proliferating epithelial cells in ulcer margin (lower panel) in different samples retrieved at day 7. *: Significantly different from the control and SIS groups ($P < 0.05$). B. Immunohistochemical staining against CD31 in granulation tissues of different samples retrieved at day 7 (left column, red arrow points positively blood vessels). Immunofluorescent staining against Ki67 in ulcer margin of the different samples retrieved at day 7 (right column; red: ki67, blue: nucleus stained with DAPI). Scale bar: 50 μm. C. Relative mRNA expression of VEGFR2, ANGPT2, COX2 and EGFR in defected gastric tissue of different groups retrieved at day 1, 3 and 7 by RT-qPCR. *: Significantly different from the control group ($P < 0.05$). #: Significantly different from the control and SIS groups ($P < 0.05$). D. VEGFR2, ANGPT2 and COX2 protein expression levels in defected gastric tissue of different groups retrieved at day 1, 3 and 7 by western blot analysis.

Discussion

Porcine SIS, approved by the U.S. Food and Drug Administration (FDA), has been broadly used in tissue engineering for its three-dimensional structure and bioactive components [31]. However, SIS, mainly made of collagen, is extremely easily degraded in gastric juice due to the existence of hydrochloric acid and pepsin, which even served as two major ingredients for the digestion of SIS to prepare gel [32]. So the application of SIS in gastric tissue repair requires effective modification. Biomaterial crosslinking strategies have been widely used to improve their strength and resistance to mechanical damage and premature degradation within challenging

View Article Online
DOI: 10.1039/C7TB00517B

environment in host [33]. Genipin, a natural crosslinking agent, has proven high efficiency in crosslinking and better biocompatibility than glutaraldehyde in previous studies [17-21]. In the present study, we employed genipin to crosslink SIS to improve its resistance against degradation in gastric juice and further explored the feasibility in improving gastric mucosa regeneration.

The crosslinking degree of biological scaffolds fixed by genipin is usually affected by different conditions [34], so firstly we optimized the conditions (temperature, time and initial crosslinking concentrations) for GP-CR SIS preparation **(Fig.S4)**. Then four different concentrations of genipin (0.05%, 0.1%, 0.3% and 0.5%) were employed to crosslink SIS at 37 $^{\circ}$C for 24 h for further study. The color of SIS changed from white to dark blue as a result of the reaction of genipin with the amino acid residues (mainly lysine, hydroxylysine and arginine) in collagen molecules [21]. The higher crosslinking degree often implies the more efficient crosslinking. Instead, the swelling ratio decreased with the high crosslinking degree, which may be attributed to the consumed hydrophilic groups and a reduction in free room to accommodate water during genipin crosslinking [35, 36]. ATR-FTIR portrayed a decrease in the characteristic peak derived from amine (-NH_2) stretch at 1549 cm^{-1} between SIS and GP-CR SIS. This can be partly attributed to the consumption of N-H and the covalent addition of carbon-carbon structures such as C-C in-ring stretch and C=C stretch, as well as the formation of amide and tertiary amine linkages within collagen through the reaction of primary amine moieties with genipin. These results indicated the efficient crosslinking of GP-CR SIS. Additionally, the crosslinking did not influence the porous structure of SIS, which guaranteed the easy adhesion and proliferation of cells on GP-CR SIS.

The rapid degradation of SIS has been observed after *in vitro* incubation in a proteolytic

View Article Online
DOI: 10.1039/C7TB00517B

solution as well as *in vivo* implantation no matter in single layer or multi-layer application [37, 38]. In the present study, we also observed a rapid degradation of SIS in SGF within 24 h. In contrast, all GP-CR SIS scaffolds remained integral, with residual mass ratios all above 90% at the end of 8-week incubation period. The huge enhancement of anti-digestive capability in GP-CR SIS scaffolds may attribute to the cleavage sites hidden or altered by the formed crosslinks. The intramolecular and intermolecular cyclic crosslinking structure of collagen in GP-CR SIS may have a great stereo-hindrance for the access of pepsin due to the huge heterocyclic-structure of genipin [39]. However, the preservation of gross appearance and surface structures were not completely consistent with changes of mechanical properties. It is reported that SIS laminates in enzyme solution lost their mechanical properties within 5 hours regardless of the maintenance of its macro appearance [38]. So the mechanical properties of GP-CR SIS scaffolds before and after the treatment of SGF were compared. Before digestion, genipin crosslinking prominently increased the ultimate tensile strength of SIS, mainly due to the denser cyclic structures introduced through intramolecular and intermolecular crosslinks combined with the hydrogen bonds formed by genipin [40]. Although the ultimate tensile strength increased with the increasing genipin concentration, the difference between GP-CR SIS groups was relatively small. This may be explained by the little variation of crosslinking degree among these scaffolds. As to the stiffness, no obvious changes can be seen between SIS and GP-CR SIS scaffolds, maybe on account of the little changes in crystalline organized domains in genipin crosslinking. After the treatment with SGF, the ultimate tensile strength declined into one fifth of its original values, presenting little variation in the subsequent treatment. This fact did not conflict with the results of residual mass ratio. Some peptide bonds between amino acids residues were opened but the peptides were still

View Article Online
DOI: 10.1039/C7TB00517B

linked to the collagen fibers by residual bonds, so the ultimate tensile stress remarkably declined while the residual mass ratio changed slightly. However, the stiffness of GP-CR SIS was less affected by the treatment of SGF, which may be ascribed to the coordinated effects that SGF exerted on the force and deformation of GP-CR SIS.

In view of the potential application of GP-CR SIS for gastric mucosa repair, human non-tumor gastric epithelial cell line GES-1 was used to evaluate the cytocompatibility of GP-CR SIS. In the direct and indirect cytotoxicity assay, GES-1 maintained good morphology and high viability whether cultured on the surface GP-CR SIS or in its extract. The better cytocompatibility of GP-CR SIS is likely due to the low cytotoxicity of genipin itself, which was about 10, 000 times less cytotoxic than glutaraldehyde [41]; and the stable and biocompatible crosslinked structures after genipin treatment, without crosslinking agent or deleterious residues released [42]. Furthermore, rather than compromise the blood compatibility of SIS, genipin crosslinking slightly promoted the hemocompatibility, which may be attributed to the lower antigenicity of GP-CR SIS. As to the histocompatibility, it is noted that the degree of inflammatory reaction implanted with SIS was serious at 1 and 2-week postimplantation. This may be caused by the remaining free amino, hydroxyl and carboxyl groups in collagen fibers and the continuous infiltration of inflammatory cells accompanied by the degradation of SIS [43-46]. With increasing implantation duration, SIS was almost completely degraded and the inflammatory response significantly declined. By contrast, the inflammatory reaction of GP-CR SIS scaffolds was relatively mild throughout the implantation. It is known that genipin may react with the free amino groups in amino acids or proteins, thus precluding the antigenic properties of collagen [17]. Additionally, the low cytotoxicity of the stable crosslinking products and the intrinsic anti-inflammatory effects of

View Article Online
DOI: 10.1039/C7TB00517B

genipin may contribute to lower inflammatory responses [47]. Furthermore, genipin crosslinking protected SIS from degradation, thus avoiding the exposure of more antigens. On the other hand, the natural biomaterials crosslinked by chemical agents, especially glutaraldehyde, often led to obvious calcification *in vivo* [48]. In our study, however, the calcium contents of GP-CR SIS scaffolds retrieved 4-week postoperatively were minimal **(Table S2),** which was consistent with the previous study [49].

In gastric mucosa repair, 0.5%GP-CR SIS was selected on account of the following two reasons. Firstly, the real environment in stomach is more challenging than SGF in view of the abrasion of the food being digested, while 0.5%GP-CR SIS provided a more stable structure based on its higher crosslinking degree. Furthermore, after being dissolved in strong acid (HCl), only 0.5%GP-CR SIS inhibited the proliferation of Helicobacter Pylori (HP) **(Fig.S5),** which is the principle cause of gastric ulcer [50]. The wound area significantly decreased in GP-CR SIS group compared with control and SIS groups at 7-day postoperatively. Rather than the formation of granulation tissue, the submucosa of control group in certain lesions was completely destroyed, even leaving muscular layer exposed after 1 week of implantation, which might result in gastric perforation. Conversely, the SIS and GP-CR SIS groups presented progressive ulcer healing with granulation tissue formation at the ulcer base, providing the “bed” for the migration of epithelium and the formation of microvessels. Obviously, the initial existence of the materials played an important role in the formation of granulation tissue, protecting the defected gastric tissue from secondary injury. However, the protection of SIS did not last long due to its degradation within 1 day, while GP-CR SIS remained intact within 14 days. Two weeks after implantation, the lesions of GP-CR SIS were covered with a continuous epithelium while the other groups had poor

View Article Online
DOI: 10.1039/C7TB00517B

re-epithelialization. Despite an almost full recovery of mucosa within 28 days, the epithelium in control and SIS groups dispersed in tubes composed of ulcer-associated cell lineage (UACL), which was closely associated with gastric ulcer healing. These tubes migrate towards the granulation tissue, appear as bud and transform into new epithelial structures [51]. Conversely, the number of tubes in GP-CR SIS group was less and most tubes have depolymerized and transformed into normal epithelial structures. To confirm the function recovery of gastric mucosa, neutral mucosubstances such as glycoproteins were stained with PAS. Most of PAS positive epithelium in GP-CR SIS group orderly aligned on the surface of mucosa like normal gastric mucosa structure and if any, few presented in tube formation. In contrast, the PAS positive cells in control and SIS groups mostly were distributed in UACL structures, indicating that they were derived from the mature epithelial cell and they involved in the ulcer healing [52]. In spite of an acceleration of GP-CR SIS in gastric mucosa regeneration, the "quality" of gastric mucosa like the thickness and the arrangement of the epithelial, still need to be ameliorated.

Besides the protective function, the growth factors in GP-CR SIS may likewise enhance the gastric mucosa healing. It has been demonstrated that the gastric ulcer healing is a programmed repair process triggered and controlled by cytokines and growth factors (e.g., VEGF, EGF, TGF-β) in partially and temporally coordinated manners [51, 52]. Additionally, growth factors in SIS are critical in fostering soft tissue repair [53, 54]. Therefore, we first analyzed the effect of genipin crosslinking on the content of VEGF and TGF-β **(Fig.S6)**, and found that genipin treatment did not affect the preservation of growth factors ($P > 0.05$). This can be explained by the mild crosslinking process and the anchoring effect provided by genipin crosslinking. Based on this, we further explored the possible mechanism of growth factors on vascularization and epithelialization.

View Article Online
DOI: 10.1039/C7TB00517B

Since the blood vessel density of GP-CR SIS group was significantly higher than the other groups at day 7 postoperatively**,** we speculated that exogenous VEGF preserved in the scaffolds contributed to the better vascularization. It has been reported that VEGF in SIS enhanced the expression of VEGFR2, a major signaling mediator in regulating endothelial cell migration and the formation of nascent vessels [55, 56]. Additionally, exogenous VEGF has been shown to up-regulate expression of ANGPT2, a downstream signal molecule of VEGFR2, which loosed the tight vascular structures and in turn facilitated the access of VEGF to endothelial cells [57, 58]. In this study, the mRNA expression of VEGFR2 and ANGPT2 were higher in GP-CR SIS and SIS groups than that in control group at day 1. On account of the rapid degradation of SIS, no prominent difference was observed between SIS and control groups in subsequent time points. Despite the increasing trend on day 3 without statistical difference compared with control and SIS groups, the mRNA expression of VEGFR2 and ANGPT2 in GP-CR SIS group remarkably increased on day 7 again, which is identified with the WB results. It has been reported that genipin crosslinking can slow the release of growth factors in biomaterials by its anchoring effect [59]. After the digestion of gastric juice for 7 days, there was an abrupt degradation in GP-CR SIS scaffold which agreed with its emergence of loosen structures. With the fall of numbers in crosslinks, the release of growth factors led to the high expression of VEGFR2 and ANPGT2 again. On the other hand, the number of proliferating epithelium in GP-CR SIS group was higher than that in control and SIS groups. This may be closely related to EGF family growth factors. It has been reported that EGF plays a pivotal role in gastric ulcer healing by modulating the proliferation and migration of epithelium [60]. Exogenous EGF prominently up-regulated COX2 expression through binding to its receptor EGFR and then accelerated the proliferation of gastric

View Article Online
DOI: 10.1039/C7TB00517B

RGM1 epithelium cells [61, 62]. It can be found that the expression of COX2 was up-regulated in GP-CR SIS group compared with that in control group within 3 days, implying the slow release of EGF from the materials. But the expression of COX2 declined to the level of control group on day 7. The function of EGF is depended on the EGFR expression, while the high expression of EGFR occurred within 3 days after gastric mucosa injury [63]. So the low expression of EGFR on day 7 may restrict the binding of exogenous EGF.

In summary, we successfully enhanced the resistance of SIS against gastric juice degradation and preserved its friendly biocompatibility by genipin crosslinking. Further, GP-CR SIS demonstrated its advantage in accelerating the defected gastric mucosa healing compared with control and SIS groups in ESD-related ulcer model. Additionally, the protective effect and the bioactivity of GP-CR SIS may play an important role in mucosa repair, while the clear mechanism needs to be studied further. Besides, this material designed for the repair of defected gastric mucosa caused by endoscopic surgery will be applied by endoscopic equipment rather than open surgery. So the delivery and the anchor of GP-CR SIS by endoscopic equipment will be explored in future study.

Conclusion

In our study, SIS was successfully modified with genipin. Crosslinking characteristics proved that genipin can effectively crosslink SIS, therefore significantly enhancing the resistance of SIS against degradation in gastric juice and its mechanical properties. Meanwhile, the cytotoxicity test, hemolysis and subcutaneous implant demonstrated that GP-CR SIS possessed good biocompatibility to support the proliferation and viability of gastric epithelial cells. *In vivo* study,

View Article Online
DOI: 10.1039/C7TB00517B

GP-CR SIS achieved great effect in accelerating the healing of defected gastric mucosa by providing protective environment and enhancing the vascularization and the re-epithelialization. Based on the aforementioned results, it is worthwhile to explore the application of GP-CR SIS in accelerating gastric mucosa regeneration through endoscopic equipment in minimal invasive surgery.

Acknowledgements

This study was supported by the National Key Research and Development Program of China (2017YFC1104702); the National Natural Science Foundation of China (31271058) and the National High Technology Research and Development Program of China (2012AA020503).

References

1 R. Soetikno, T. Kaltenbach, R. Yeh and T. Gotoda, *J. Clin. Oncol.,* 2005, **23**, 4490.

2 S. Oka, S. Tanaka, I. Kaneko, R. Mouri, M. Hirata, T. Kawamura, M. Yoshihara and K. Chayama, *Gastrointest. Endosc.,* 2006, **64**, 877

3 T, Kojima, A. Parra-Blanco, H. Takahashi and R. Fujita, *Gastrointest. Endosc.*, 1998, **8**, 550.

4 B. Andrée, A. Bär, A. Haverich and A. Hilfiker, *Tissue Eng., Part B,* 2013, **19**, 279.

5 W. Jiang, J. Zhang, X. Lv, C. Lu, H. Chen, X. Xu and W. Tang, *J. Pediatr. Surg.,* 2016, **51**, 368

6 S. L. Voytik-Harbin, A. O. Brightman, M. R. Kraine, B. Waisner and S. F. Badylak, *J. Cell Biochem.,* 1997, **67**, 478.

7 J. P. Hodde, S. F. Badylak, A. O. Brightman and S. L. Voytik-Harbin, *Tissue Eng.,* 1996, **2**,

View Article Online
DOI: 10.1039/C7TB00517B

209

8 T. B. McPherson and S. F. Badylak, *Tissue Eng.,* 1998, 4, 75.

9 R. G. Witt, G. Raff, J. Van Gundy, M. Rodgers-Ohlau and M. S. Si, *Eur. J. Cardiothorac. Surg.,* 2013, **44**, 72.

10 H. K. Lin, S. Y. Godiwalla, B. Palmer, D. Frimberger, Q. Yang, S. V. Madihally, K. M. Fung and B. P. Kropp, *Tissue Eng., Part B*, 2014, **20**, 73.

11 M. S. Kim, K. D. Hong, H. W. Shin, S. H. Kim, S. H. Kim, M. S. Lee, W. Y. Jang, G. Khang and H. B. Lee, *Int. J. Biol. Macromol.*, 2005, **36**, 54.

12 S. Wu, Y. Liu, S. Bharadwaj, A. Atala and Y. Zhang, *Biomaterials,* 2011, **32**, 1317..

13 M. Rosen, J. Ponsky, R. Petras, A. Fanning, F. Brody and F. Duperier, *Surgery*, 2002, **132**, 480.

14 G. M. Gunning and B. P. Murphy, *J. Mech. Behav. Biomed. Mater.,* 2016, **57**, 321.

15 N. Fukunaga, T. Matsuo, Y. Saji, Y. Imai and T. Koyama, *Ann. Thorac. Surg.,* 2015, **99**, 2203.

16 A. J. Kuijpers, G. H. Engbers, J. Krijgsveld, S. A. Zaat, J. Dankert and J. Feijen, *J. Biomater. Sci. Polym. Ed.,* 2000, **11**, 225.

17 L. L. Huang, H. W. Sung, C. C. Tsai and D. M. Huang, *J. Biomed. Mater. Res.,* 1998, **42**, 568.

18 F. L. Mi, Y. C. Tan, H. F. Liang and H. W. Sung, *Biomaterials,* 2002, **23**, 181.

19 Y. S. Chen, J. Y. Chang, C. Y. Cheng, F. J. Tsai, C. H. Yao and B. S. Liu, *Biomaterials*, 2005, **26**, 3911.

20 S. A. Sell, M. P. Francis, K. Garg, M. J. McClure, D. G. Simpson and G. L. Bowlin, *Biomed. Mater.*, 2008, **3**, 045001.

View Article Online
DOI: 10.1039/C7TB00517B

21 H. W. Sung, R. N. Huang, L. L. Huang, C. C. Tsai and C. T. Chiu, *J. Biomed. Mater. Res.,* 1998, **42**, 560.

22 H. W. Sung, C. S. Hsu, S. P. Wang and H. L. Hsu, *J. Biomed. Mater. Res.,* 1997, **35**, 147.

23 H. W. Sung, Y. Chang, C. T. Chiu, C. N. Chen and H. C. Liang, *J. Biomed. Mater. Res*., 1999, **47**, 116.

24 Z. Liu, Q. Zhou, J. Zhu, J. Xiao, P. Wan, C. Zhou, Z. Huang, N. Qiang, W. Zhang, Z. Wu, D. Quan and Z. Wang, *Biomaterials,* 2012, **33**, 7336.

25 J. C. Luo, W. Chen, X. H. Chen, T. W. Qin, Y. C. Huang, H. Q. Xie, X. Q. Li, Z. Y. Qian and Z. M. Yang, *Biomaterials*, 2011, **32**, 706.

26 R. Meena, K. Prasad and A. K. Siddhanta, *J. Appl. Polym. Sci.,* 2007, **104**, 290.

27 S. Nakatsuka and A. L. Andrady, *J. Appl. Polym. Sci.,* 1992, **44**, 17.

28 F. L. Mi, *Biomacromolecules*, 2005, **6**, 975.

29 S. Okabe, J. L. Roth and C. J. Pfeiffer, *J. Dig. Dis*., 1971, **16**, 277.

30 K. Burugapalli and A. Pandit, *Biomacromolecules*, 2007, **8**, 3439.

31 S. F. Badylak, D. O. Freytes and T. W. Gilbert, *Acta Biomater*, 2009, **5**, 1.

32 R. E. Hurst, P. J. Hauser, K. D. Kyker, J. E. Heinlen, J. P. Hodde, M. C. Hiles, S. D. Kosanke, M. Dozmorov and M. A. Ihnat, *PLoS One*, 2013, **8**, e64181.

33 G. Fessel, J. Cadby, S. Wunderli, R. van Weeren and J. G. Snedeker, *Acta Biomater*., 2014, **10**, 1897.

34 H. W. Sung, Y. Chang, I. L. Liang, W. H. Chang and Y. C. Chen, *J. Biomed, Mater. Res*., 2000, **52**, 77.

35 L. P. Yan, Y. J. Wang, L. Ren, G. Wu, S. G. Caridade, J. B. Fan, L. Y. Wang, P. H. Ji, J. M.

View Article Online
DOI: 10.1039/C7TB00517B

Oliveira, J. T. Oliveira, J. F. Mano and R. L. Reis, *J. Biomed, Mater. Res*., 2010, **95**, 465.

36 J. N.Hiremath and B. Vishalaksh, *Der. Pharma, Chemica*., 2012 , **4**, 946.

37 S. F. Badylak, B. Kropp, T. McPherson, H. Liang and P. W. Snyder, *Tissue Eng*., 1998, **4**, 379.

38 R. Mewaldt, L. Shi and D. Carson, *Wound Repair & Regeneration*, 2011, **19**, A39.

39 F. L. Mi, Y. C. Tan, H. C. Liang, R. N. Huang and H. W. Sung, *J. Biomater. Sci. Polym. Ed*., 2001, **12**, 835.

40 H. W. Sung, Y. Chang, C. T. Chiu, C. N. Chen and H. C. Liang, *J. Biomed. Mater. Res*., 1999, **47**, 116.

41 H. W. Sung, R. N. Huang, L. L. Huang and C. C. Tsai, *Biomater. Sci. Polym. Ed*., 1999, **10**, 63.

42 H. W. Sung, I. L. Liang, C. N. Chen, R. N. Huang and H. F. Liang, *J. Biomed. Mater. Res*., 2001, **55**, 538.

43 E. Khor, *Biomaterials*, 1997, **18**, 95.

44 P. B. van Wachem, M. J. van Luyn, L. H. Olde Damink, P. J. Dijkstra, J. Feijen and P. Nieuwenhuis, *Int. J. Artif. Organs*, 1994, **17**, 230.

45 S. D. Gorham, T. P. Hyland, D. A. French and M. J. Willins, *Biomaterials*, 1990, **11**, 113.

46 R. Scott, R. Baraza, S. D. Gorham, I. McGregor and D. A. French, *Br. J. Urol*., 1986, **58**, 203.

47 H. J. Koo, Y. S. Song, H. J. Kim, Y. H. Lee, S. M. Hong, S. J. Kim, B. C. Kim, C. Jin, C. J. Lim and E. H. Park, *Eur. J. Pharmacol*., 2004, **495**, 201.

48 H. G. Lim, S. H. Kim, S. Y. Choi and Y. J. Kim, *Eur. J. Cardiothorac. Surg*., 2012, **41**, 383.

View Article Online
DOI: 10.1039/C7TB00517B

49 Y. Chang, M. H. Lee, H. C. Liang, C. K. Hsu and H. W. Sung, *Tissue Eng*., 2004, **10**, 881.

50 N. F. Tanih, L. M. Ndip, A. M. Clarke and R. N. Ndip, *Afr. J. Microbiol. Res*., 2010, **4**, 426.

51 A. S. Tarnawski, *Dig. Dis. Sci*., 2005, **50**, 24.

52 A. F. Syam, M. Sadikin, S. I. Wanandi and A. A. Rani, *Indones*., 2009, **41**, 95.

53 J. H. Spiegel and T. J. Egan, *Surg*., 2004, **30**, 1486.

54 R. M. Smith, C. Wiedl, P. Chubb and C. H. Greene, *J. Invest. Surg*., 2004, **17**, 339.

55 W. Wang, X. Zhang, N. N. Chao, T. W. Qin, Y. Zhang, J. W. Sang and J. C. Luo, *Acta Biomater*., 2016, **29**, 135.

56 A. Gampel, L. Moss, M. C. Jones, V. Brunton, J. C. Norman and H. Mellor, *Blood*, 2006, **108**, 2624.

57 H. Oh, H. Takagi, K. Suzuma, A. Otani, M. Matsumura and Y. Honda, *J. Biol. Chem*., 1999, **274**, 15732.

58 K. Teichert-Kuliszewska, P. C. Maisonpierre, N. Jones, A. I. Campbell, Z. Master, Z. Bendeck, K. Alitalo, D. J. Dumont, G. D. Yancopoulos and D. J. Stewart, *Cardiovasc. Res*., 2001, **49**, 659.

59 L. Solorio, C. Zwolinski, A. W. Lund, M. J. Farrell and J. P. Stegemann, *J. Tissue. Eng. Regen. Med*., 2010, **4**, 514.

60 A. S. Tarnawski and A. Ahluwalia, *Curr. Med. Chem*., 2012, **19**, 16.

61 J. W. Konturek, T. Brzozowski and S. J. Konturek, *J. Clin. Gastroenterol*., 1991, **13**, 88.

62 E. Sasaki, K. Tominaga, T. Watanabe, Y. Fujiwara, N. Oshitani, K. Higuchi, A. S. Tarnawski and T. Arakawa, *Dig. Dis. Sci*., 2003, **48**, 2257.

63 G. H. Choi, H. S. Park, K. R. Kim, K. R. Choi, K. T. Jang, M. J. Chung, M. J. Kang, D. G.

View Article Online
DOI: 10.1039/C7TB00517B

Lee and W. S. Moon, *Mol. Med. Rep*., 2008, **1**, 505.